Global Passivity Enforcement Algorithm for Macromodels of Interconnect Subnetworks Characterized by Tabulated Data

Dharmendra Saraswat, *Student Member, IEEE*, Ramachandra Achar, *Senior Member, IEEE*, and Michel S. Nakhla, *Fellow, IEEE*

***Abstract*—With the continually increasing operating frequencies, complex high-speed interconnect and package modules require characterization based on measured/simulated data. Several algorithms were recently suggested for macromodeling such types of data to enable unified transient analysis in the presence of external network elements. One of the critical issues involved here is the passivity violations associated with the computed macromodel. To address this issue, a new passivity enforcement algorithm is presented in this paper. The proposed method adopts a global approach for passivity enforcement by ensuring that the passivity correction at a certain region does not introduce new passivity violations at other parts of the frequency spectrum. It also provides an error estimate for the response of the passivity corrected macromodel.**

***Index Terms*—High-speed interconnects, measured subnetworks, passive macromodels, positive real system, signal integrity, system identification, tabulated data.**

I. Introduction

CHARACTERIZATION and simulation of linear subnetworks based on tabulated data has become a topic of intense research during the recent years [1]–[21]. The tabulated data can be obtained either directly from measurements or from rigorous full-wave electromagnetic simulations. Important applications of such a characterization include high-speed interconnects, packages, vias, nonuniform transmission lines, on-chip passive components, and high-frequency microwave devices. Transient simulation of such frequency-dependent *tabulated* data in the presence of nonlinear devices is a CPU-intensive process due to the mixed frequency–time problem. This can be addressed by approximating the tabulated data by rational functions and subsequently synthesizing a SPICE-compatible macromodel/netlist from such an approximation. However, the primary challenge here is to ensure the passivity of the macromodel. Passivity is an important property [22]–[25], because stable but nonpassive models may lead to unstable systems when connected to other passive components.

Several macromodeling and passivity preservation algorithms for tabulated data can be found in the literature [1]–[16]. Algorithms such as the ones based on convex optimization [15] can guarantee the passivity of the macromodel. However, they can be CPU intensive (since the associated computational complexity is in the range of n^5 to n^6, where n is the order of the state–space matrix) and may not be practically feasible. On the other hand, approaches such as the ones in [1]–[10] are computationally fast. However, they may not strictly guarantee the macromodel passivity. Hence, for such class of algorithms it becomes essential to verify the macromodel passivity and correct for any passivity violations.

In case of any passivity violations, several algorithms to enforce passivity were recently proposed [17]–[21]. These algorithms take a local approach for passivity enforcement by attempting to correct passivity violation at a particular region, without concerning the rest of the frequency spectrum.

One of the major limitations of these algorithms is that any attempt for passivity correction at some frequency point may lead to new passivity violation at other frequency points. In order to address this problem, a global passivity enforcing algorithm is presented in this paper. The new algorithm employs a guaranteed search direction for enforcing passivity, such that the correction for passivity at a certain frequency region does not introduce new regions of passivity violation.

The remainder of the paper is organized as follows. Sections II and III present the problem formulation and discuss passivity verification algorithms, respectively. Section IV describes the proposed passivity enforcement algorithm. Sections V and VI present computational results and conclusions, respectively.

II. Problem Formulation

The tabulated data can be multi-port scattering (S), admittance (Y), impedance (Z), transmission (T), or hybrid (H) parameters. Without loss of generality, in this paper it is assumed that the frequency-domain Y parameter data is given. The admittance matrix of a m-port subnetwork can be written in terms of a pole-residue formulation as

$$\boldsymbol{Y}(s) = [Y_{ij}(s)];\ Y_{ij}(s) = c^{i,j} + \sum_{q=1}^{N} \frac{k_q^{i,j}}{s - p_q};\ (i,j \in 1 \ldots m) \tag{1}$$

where the residues (k_q) and poles (p_q) can be real or complex conjugate pairs, N is the total number of poles, and c represents the direct coupling constant. Next, the state–space representation for (1) can be obtained as [26]–[28]

$$\begin{aligned} \dot{\boldsymbol{x}}(t) &= \boldsymbol{A}\boldsymbol{x}(t) + \boldsymbol{B}\boldsymbol{u}(t) \\ \boldsymbol{y}(t) &= \boldsymbol{C}\boldsymbol{x}(t) + \boldsymbol{D}\boldsymbol{u}(t). \end{aligned} \tag{2}$$

Manuscript received September 10, 2003; revised March 14, 2005.

The authors are with the Department of Electronics, Carleton University, Ottawa, ON K1S 5B6, Canada (e-mail: achar@doe.carleton.ca).

Digital Object Identifier 10.1109/TVLSI.2005.850098

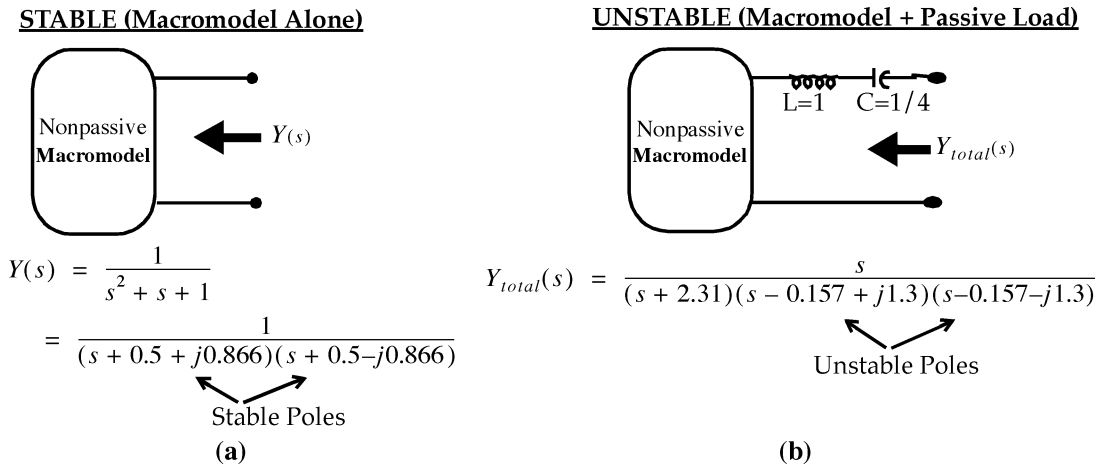

Fig. 1. Illustration of significance of passivity. (a) Stable macromodel. (b) Unstable system (macromodel + load).

Here, $\boldsymbol{A} \in \Re^{n\times n}$, $\boldsymbol{B} \in \Re^{n\times m}$, $\boldsymbol{C} \in \Re^{m\times n}$, $\boldsymbol{D} \in \Re^{m\times m}$, $\boldsymbol{u}(t) \in \Re^m$, $\boldsymbol{y}(t) \in \Re^m$, and n is the total number of state variables. It is to be noted that the poles of the system are contained in matrix $\boldsymbol{A}$ and residues in matrix $\boldsymbol{C}$ (referred to as the residue matrix). It should be noted that $\boldsymbol{D}$ contains dc coupling terms, which may not necessarily be present in all networks. The transfer function of the system relating the input $\boldsymbol{u}(t)$ to the output $\boldsymbol{y}(t)$ can be obtained as

$$\boldsymbol{Y}(s) = \boldsymbol{C}(s\boldsymbol{I} - \boldsymbol{A})^{-1}\boldsymbol{B} + \boldsymbol{D}. \tag{3}$$

Several methods have been suggested in the literature, which start with the tabulated data to obtain the macromodel of (2) and (3) via rational function approximation. While these methods may generate accurate approximations, the passivity of the resulting macromodel is not guaranteed. However, as mentioned in the introduction, the loss of passivity can be a serious problem because transient simulations of a stable but nonpassive macromodel may encounter artificial oscillations.

On the other hand, a passive macromodel, when terminated with any arbitrary passive load, always guarantees the stability of the overall resulting network. To illustrate this point, consider a simple, single-port second-order macromodel shown in Fig. 1(a). The macromodel is stable but not passive. When this macromodel is terminated with the passive load [Fig. 1(b)], the overall network ends up having unstable poles.

Therefore, the challenge here is to ensure passivity of the multiport macromodel. The conditions for a network with admittance matrix $\boldsymbol{Y}(s)$ to be passive are [29]–[31]

a) $\boldsymbol{Y}(s^*) = \boldsymbol{Y}^*(s)$, where "*" is the complex conjugate operator.

b) $\boldsymbol{Y}(s)$ is a positive real (PR) matrix, i.e., the product $\boldsymbol{z}^{*t}[\boldsymbol{Y}^t(s^*) + \boldsymbol{Y}(s)]\boldsymbol{z} \geq 0$ for all complex values of s with $Re(s) > 0$ and any arbitrary vector $\boldsymbol{z}$.

Condition a) is automatically satisfied since the complex poles/residues of the transfer function are always considered along with their conjugates, leading to only real coefficients in rational functions of $\boldsymbol{Y}(s)$. However, ensuring condition b) is not easy. For the practical case of networks with symmetric admittance matrices, condition b) can also be expressed using (3) as

$$\begin{aligned}&\text{Real}\,(\boldsymbol{Y}(j\omega))\\ &\quad = \boldsymbol{F}(j\omega)\\ &\quad = -\boldsymbol{C}\boldsymbol{A}(\omega^2\boldsymbol{I}+\boldsymbol{A}^2)^{-1}\boldsymbol{B}+\boldsymbol{D}\geq 0, \quad \text{for } \omega\in\Re\cup\infty.\end{aligned} \tag{4}$$

Equation (4) also implies that all the eigenvalues of $\boldsymbol{F}(j\omega)$ must be greater than zero for $\omega \in \Re\cup\infty$ [30]. Ensuring (4) could be a challenging task for macromodels obtained from tabulated data. Straightforward application of passivity constraints can lead to a nonlinear optimization problem. Recent approaches use CPU-efficient formulation by enforcing passivity conditions for a certain frequency region or on only given (specific) data points or through some linearized passivity constraints [1]–[10]. Although these algorithms are computationally fast, they do not guarantee the macromodel passivity. Hence, passivity verification and correction becomes crucial for guaranteeing the stability of transient simulations involving such macromodels and the rest of the network. The next section discusses the macromodel passivity verification.

III. Passivity Verification

The traditional method for macromodel passivity verification is based on a frequency sweep of eigenvalues of the real part of the admittance matrix (Real($\boldsymbol{Y}(j\omega)$)). However, this approach suffers from several drawbacks, such as up to what frequency to sweep and how fine the sweep should be. In addition, it fails to identify the exact locations of violation (which are vital for a successful compensation). In order to address these issues, the following two theorems are used, which enable systematic passivity verification without resorting to frequency-sweep.

Theorem 1: The state–space system $(\boldsymbol{A}, \boldsymbol{B}, \boldsymbol{C}, \boldsymbol{D})$ is passive if the following Hamiltonian matrix $(\boldsymbol{M})$ [32] has no imaginary eigenvalues:

$$\boldsymbol{M} = \begin{bmatrix} \boldsymbol{A} - \boldsymbol{B}(\boldsymbol{D}+\boldsymbol{D}^t)^{-1}\boldsymbol{C} & \boldsymbol{B}(\boldsymbol{D}+\boldsymbol{D}^t)^{-1}\boldsymbol{B}^t \\ -\boldsymbol{C}^t(\boldsymbol{D}+\boldsymbol{D}^t)^{-1}\boldsymbol{C} & -\boldsymbol{A}^t + \boldsymbol{C}^t(\boldsymbol{D}+\boldsymbol{D}^t)^{-1}\boldsymbol{B}^t \end{bmatrix}. \tag{5}$$

The advantage of this theorem is that the formulation of the Hamiltonian matrix is independent of frequency. Hence, if no imaginary eigenvalues are found, it automatically implies that the macromodel is passive. However, using the traditional method of frequency-sweep of eigenvalues of $\boldsymbol{F}(j\omega)$ (defined in (4)) would have required the sweep from 0 to ∞ to detect if the eigenvalues are negative at any frequency. In addition, while using the traditional method, there would be no guarantee of detecting such cases, as it depends on the fineness of the sweep (interval between frequency points during the sweep).

If the macromodel is nonpassive, it needs to be corrected (compensated for passivity violation). For a successful and fast compensation, it is essential to know the exact frequency locations at which eigenvalues of $\boldsymbol{F}(j\omega)$ cross over from a positive value to a negative value. For this purpose, the following theorem [19]–[21], [33] is used.

Theorem 2: The real part of the symmetric admittance matrix $\boldsymbol{F}(j\omega_0)$ is singular if $j\omega_0$ is an eigenvalue of the corresponding Hamiltonian matrix $\boldsymbol{M}$, provided $\boldsymbol{D}+\boldsymbol{D}^t$ is a positive definite matrix.

Theorem 2 implies that an imaginary eigenvalue of the Hamiltonian matrix $\boldsymbol{M}$ corresponds to the frequency at which $\boldsymbol{F}(j\omega)$ becomes singular (i.e., the macromodel becomes nonpassive). This information of exact locations where an eigenvalue of $\boldsymbol{F}(j\omega)$ becomes zero is very crucial as its knowledge helps the passivity compensation process. The proof of Theorem 2 can be found in [7], and a proof of its corollary is given in the Appendix. The next section describes a new passivity compensation (correction) algorithm for macromodels having passivity violations. It is assumed that the macromodel is asymptotically passive at $\omega=\infty$ (i.e., $\boldsymbol{D}+\boldsymbol{D}^t>0$), which can be easily ensured using algorithms such as [17].

IV. Passivity Enforcement

As discussed in the introduction, several algorithms [17]–[21] were recently proposed to enforce passivity in macromodels with small violations. However, these algorithms suffer from the limitation that the passivity violation may be introduced at some other frequency points while performing correction in a certain frequency region. In order to overcome this difficulty, a new algorithm is presented in this section. This algorithm employs a guaranteed search direction for enforcing passivity, such that the correction for passivity in a certain frequency region does not introduce new regions of passivity violation. The proposed method performs compensation by refining only few selected elements of the residue matrix $\boldsymbol{C}$ of the state–space system. These elements are selected from the real part of residues of diagonal elements of $\boldsymbol{Y}(s)$, corresponding to the poles in the vicinity of passivity violation. The proposed passivity enforcement algorithm consists of the following three steps:

1) determination of passivity violation regions;
2) determination of the magnitude of the maximum violation in a given nonpassive region;
3) performance of passivity correction by perturbing the selected residues.

The details of these steps are given in the following subsections.

A. Determination of Passivity Violation Regions

It is known from Theorem 2 that the imaginary eigenvalues of the Hamiltonian matrix $\boldsymbol{M}$ of (5) correspond to the frequency locations where the Real$(\boldsymbol{Y}(j\omega))=\boldsymbol{F}(j\omega)$ becomes singular. However, this information does not tell us anything about the regions of passivity violation (i.e., the frequency bandwidth in which an eigenvalue of $\boldsymbol{F}(j\omega)$ is negative). In order to determine the regions of passivity violation, we determine the slope of eigenvalues of $\boldsymbol{F}(j\omega)$ at its singular locations. This is done as follows.

If λ is an eigenvalue of $\boldsymbol{F}(j\omega)$ and $\boldsymbol{u}$ the corresponding right eigenvector, then we have

$$(\boldsymbol{F}(j\omega)-\lambda\boldsymbol{I})\,\boldsymbol{u}=0. \tag{6}$$

Differentiating this equation with respect to the angular frequency ω

$$\left(\frac{d}{d\omega}\boldsymbol{F}(j\omega)-\frac{d\lambda}{d\omega}\boldsymbol{I}\right)\boldsymbol{u}+(\boldsymbol{F}(j\omega)-\lambda\boldsymbol{I})\,\frac{d\boldsymbol{u}}{d\omega}=0. \tag{7}$$

Next, multiplying (7) by the left eigenvector $(\boldsymbol{v}^t)$ of $\boldsymbol{F}(j\omega)$

$$\boldsymbol{v}^t\frac{d}{d\omega}\boldsymbol{F}(j\omega)\boldsymbol{u}-\boldsymbol{v}^t\frac{d}{d\omega}(\lambda)\boldsymbol{u}+\underbrace{\boldsymbol{v}^t\,(\boldsymbol{F}(j\omega)-\lambda\boldsymbol{I})}_{=0}\frac{d\boldsymbol{u}}{d\omega}=0. \tag{8}$$

Notice that the last term on the left-hand side of (8) is zero by the definition of left eigenvector. Using this fact, (8) can be rewritten as

$$\boldsymbol{v}^t\frac{d}{d\omega}(\lambda)\boldsymbol{u}=\boldsymbol{v}^t\frac{d}{d\omega}\boldsymbol{F}(j\omega)\boldsymbol{u} \tag{9}$$

or

$$\frac{d\lambda}{d\omega}=\frac{\boldsymbol{v}^t\frac{d}{d\omega}\boldsymbol{F}(j\omega)\boldsymbol{u}}{\boldsymbol{v}^t\boldsymbol{u}}. \tag{10}$$

Next, the derivative of $\boldsymbol{F}(j\omega)$ with respect to ω can be obtained using (4) as

$$\frac{d}{d\omega}\boldsymbol{F}(j\omega)=\boldsymbol{C}\boldsymbol{A}(\omega^2\boldsymbol{I}+\boldsymbol{A}^2)^{-2}2\omega\boldsymbol{B}. \tag{11}$$

Substituting (11) into (10), we get

$$\frac{d\lambda}{d\omega}=\frac{\boldsymbol{v}^t\left(\boldsymbol{C}\boldsymbol{A}(\omega^2\boldsymbol{I}+\boldsymbol{A}^2)^{-2}2\omega\boldsymbol{B}\right)\boldsymbol{u}}{\boldsymbol{v}^t\boldsymbol{u}}. \tag{12}$$

Using (12), we can determine the slope of eigenvalues of $\boldsymbol{F}(j\omega)$ at its singular frequencies. The regions and bandwidth of local passivity violation are then determined using the following steps.

1) Collect the pure imaginary eigenvalues (consider only those with positive imaginary parts) of the Hamiltonian matrix $\boldsymbol{M}$ of (5) in a vector $\boldsymbol{S_a}=[\omega_1,\omega_2\ldots\omega_T]$ such that $\omega_1<\omega_2<\ldots<\omega_T$, where "$T$" is the total number of such entries. Let $\omega_H=\omega_T$.

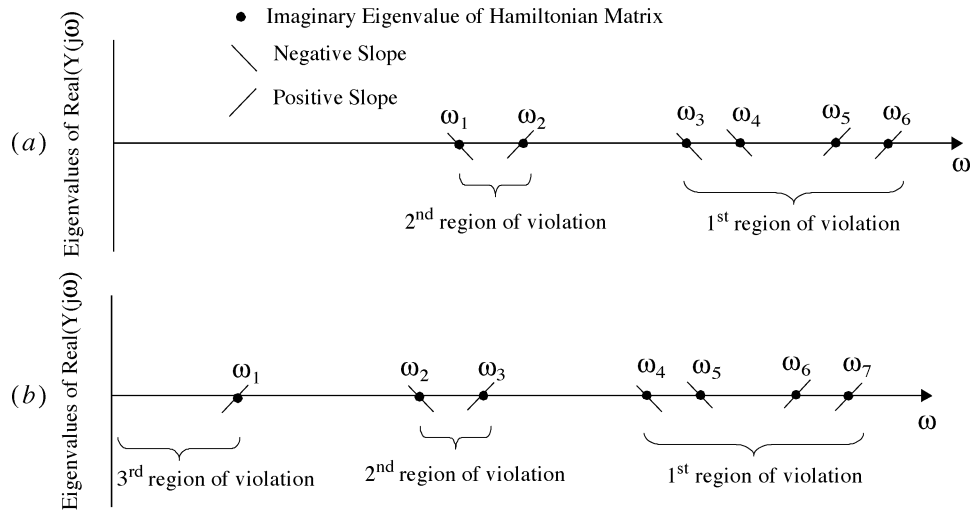

Fig. 2. Illustration of identification of regions of passivity violation.

It should be noted that finding the imaginary eigenvalue may not be a trivial task, since the real part of the eigenvalue may not be equal to zero, owing to the presence of numerical noise. In our implementation, this difficulty is overcome by using the property of the Hamiltonian matrix, that is, its eigenvalue spectrum is symmetric with reference to both the real as well as the imaginary axis. This implies that if λ is a complex eigenvalue of a given Hamiltonian matrix, then $-\lambda$, λ^*, and $-\lambda^*$ are also its eigenvalues. On the other hand, the imaginary eigenvalues are symmetric only with respect to the real axis (i.e., if λ is an imaginary eigenvalue of a given Hamiltonian matrix, then $-\lambda$ is also its eigenvalue). As a consequence of this property, while determining if an eigenvalue is imaginary or not, we check for the eigenvalues, which are symmetric only about the real axis. As a result, the effect of numerical noise is taken care of while identifying the imaginary eigenvalues of the Hamiltonian matrix.

2) Next, at the frequency corresponding to each of the above entries, evaluate the slope of the eigenvalue of $\boldsymbol{F}(j\omega)$ using (12). Note that the slope at ω_T is always positive since $\boldsymbol{D}+\boldsymbol{D}^t > 0$.
3) Count the number of positive and negative slopes starting from ω_H. When the count of positive and negative slopes become equal, say at ω_k, then the first region of local passivity violation is established (i.e., the region between ω_H to ω_k).
4) Reset the count of slope to zero and designate $\omega_H = \omega_{k-1}$ and repeat Steps 3 and 4 until all entries in the vector $\boldsymbol{S_a}$ are exhausted.

These steps are illustrated in Fig. 2(a), for the case of Hamiltonian matrix having six pairs of imaginary eigenvalues.

The situation when the passivity violation starts at zero frequency is illustrated with an example in Fig. 2(b). As seen in this example, when the counting of slopes is restarted after determining the second region of violation, the number of positive slopes becomes one and the number of negative slopes is equal to zero, at the end of counting the slopes. In such cases, a region of violation exists between the first frequency point from where the counting of slope is restarted (in this case, ω_1) and zero Hertz (origin).

The proposed passivity enforcement algorithm assumes that the imaginary eigenvalues of the Hamiltonian matrix are simple. However, it can be easily extended to the case of Hamiltonian matrices with repeated imaginary eigenvalues using the well-established approach outlined in [20].

B. Determination of Magnitude of the Maximum Violation in a Nonpassive Region

In this step, the exact location of maximum passivity violation (i.e., the maximum negative eigenvalue of $\boldsymbol{F}(j\omega)$) is determined in each region of passivity violation (these locations are corrected first during the compensation process). These locations are found by solving the following problem in each region of passivity violation:

$$\min_{\omega} \operatorname{eig}\left(\operatorname{Real}\left(Y(j\omega)\right)\right) \qquad \omega \in \omega_l, \omega_h \tag{13}$$

where ω_l and ω_h are the boundaries of a passivity violating region. For instance, in the first region of violation in Fig. 2(a), $\omega_l = \omega_3$ and $\omega_h = \omega_6$. The problem in (13) converges very fast as it is associated with only one variable (ω) and has a good initial guess (midpoint of ω_l and ω_h).

C. Passivity Compensation

With the regions of passivity violation as well as location and magnitude of maximum violations in each such region known, the passivity correction (compensation) is performed as follows. Consider the real part of the admittance matrix, given by (4). If the macromodel is nonpassive (i.e., $\boldsymbol{F}(j\omega)$ is negative definite), we perturb the residue matrix $\boldsymbol{C}$ by $\Delta\boldsymbol{C}$ (keeping matrices $\boldsymbol{A}$, $\boldsymbol{B}$, and $\boldsymbol{D}$ unchanged) so that

$$\boldsymbol{F}(j\omega) + \Delta\boldsymbol{F}(j\omega) = -(\boldsymbol{C}+\Delta\boldsymbol{C})\boldsymbol{A}(\omega^2\boldsymbol{I}+\boldsymbol{A}^2)^{-1}\boldsymbol{B}+\boldsymbol{D} \geq 0 \tag{14}$$

at the frequency point of maximum violation in a nonpassive region under consideration. For example, let $-\Delta\lambda$ represent the eigenvalue of $\boldsymbol{F}(j\omega)$ at a frequency point of

maximum passivity violation. To compensate this, we add $\Delta\bar{\boldsymbol{F}}(j\omega) = -\Delta\boldsymbol{C}\boldsymbol{A}(\omega^2\boldsymbol{I}+\boldsymbol{A}^2)^{-1}\boldsymbol{B}$ to $\bar{\boldsymbol{F}}(j\omega)$ by slightly perturbing the matrix $\boldsymbol{C}$ such that [34]

$$\Delta\lambda = \frac{\boldsymbol{y}^t\Delta\boldsymbol{F}(j\omega)\boldsymbol{x}}{\boldsymbol{y}^t\boldsymbol{x}} = \frac{-\boldsymbol{y}^t\Delta\boldsymbol{C}\boldsymbol{A}(\omega^2\boldsymbol{I}+\boldsymbol{A}^2)^{-1}\boldsymbol{B}\boldsymbol{x}}{\boldsymbol{y}^t\boldsymbol{x}} \tag{15}$$

where $\boldsymbol{y}$ and $\boldsymbol{x}$ are the left and right eigenvectors of $\boldsymbol{F}(j\omega)$. After some algebraic manipulations, (15) can be converted into a set of linear equations in the form

$$\Delta\lambda = \Theta\boldsymbol{Q} \tag{16}$$

where the unknown perturbed values of selected residues are contained in the vector $\boldsymbol{Q}$. Next, details on the selection of appropriate residues for perturbation to achieve the desired correction is given.

1) Selection of Appropriate Residues for Perturbation: In the proposed algorithm, the perturbation is effected on real part of residues of driving point admittances corresponding to the poles in the vicinity of passivity violation. Identification of such poles is done by determining the contribution of each pole to the real part of diagonal elements of the admittance matrix in the frequency region of violation. This is done by integrating the square of the real part of the response (represented by $R(\omega)$) of every pole for a passivity violating region under consideration (with boundaries ω_1 and ω_2), as follows:

$$\int_{\omega_1}^{\omega_2} \left(R(\omega)\right)^2 d\omega. \tag{17}$$

The poles with the significant contribution are selected, and their residues corresponding to the driving point admittances are perturbed during passivity compensation process. Next, an appropriate mapping of such residues to the residue matrix $\boldsymbol{C}$ (for formulating $\Delta\boldsymbol{C}$ and $\boldsymbol{Q}$ of (14) and (16), respectively) is illustrated using the following example.

Consider a two-port network with two poles $p_1 = w+jz$ and $p_2 = w-jz$. Let the corresponding residues at different ports be $c_{k,l} = (r \pm jg)_{k,l}$; $k,l = 1,2$. The state–space realization [26]–[28] for the network can be expressed as

$$\begin{bmatrix}\dot{x}_1\\ \dot{x}_2\\ \dot{x}_3\\ \dot{x}_4\end{bmatrix} = \underbrace{\begin{bmatrix} w & 0 & z & 0\\ 0 & w & 0 & z\\ -z & 0 & w & 0\\ 0 & -z & 0 & w\end{bmatrix}}_{\boldsymbol{A}}\begin{bmatrix}x_1\\ x_2\\ x_3\\ x_4\end{bmatrix} + \underbrace{\begin{bmatrix}2 & 0\\ 0 & 2\\ 0 & 0\\ 0 & 0\end{bmatrix}}_{\boldsymbol{B}}\begin{bmatrix}v_1\\ v_2\end{bmatrix}. \tag{18}$$

Assuming that the above poles are identified by (17), the residues shown in the following equation are perturbed in the proposed algorithm:

$$\boldsymbol{y} = \begin{bmatrix}i_1\\ i_2\end{bmatrix} = \underbrace{\begin{bmatrix} r_{11} & r_{12} & g_{11} & g_{12}\\ r_{21} & r_{22} & g_{21} & g_{22}\end{bmatrix}}_{\boldsymbol{C}}\begin{bmatrix}x_1\\ x_2\\ x_3\\ x_4\end{bmatrix} \tag{19}$$

Consequently, $\Delta\boldsymbol{C}$ for this example can be represented as

$$\Delta\boldsymbol{C} = \begin{bmatrix}\Delta r_{11} & 0 & 0 & 0\\ 0 & \Delta r_{22} & 0 & 0\end{bmatrix} \tag{20}$$

and the corresponding unknown vector $\boldsymbol{Q}$ in (16) is $\boldsymbol{Q} = [\Delta r_{11}\ \Delta r_{22}]$. For the general case of the m-port network with n pair of complex poles, if the l^{th} pole pair is selected by (17), then the corresponding $\Delta\boldsymbol{C}$ has the form shown in (21) at bottom of page, and the corresponding unknown vector $\boldsymbol{Q}$ in (16) is $\boldsymbol{Q} = [\Delta r_{11}^l\ \Delta r_{22}^l \ldots \Delta r_{mm}^l]$. In case more poles are involved, then $\Delta\boldsymbol{C}$ will have block diagonal entries for the corresponding poles similar to the one described by (21), and vector $\boldsymbol{Q}$ is formulated accordingly.

With the residues for perturbation selected as per above guidelines, (16) is solved to offset $-\Delta\lambda$ (obtained as per the guidelines in Section IV-B), the eigenvalue of $\boldsymbol{F}(j\omega)$ at the frequency point of maximum violation. This process is continued at the point of maximum passivity violation in each passivity violation regions.

The advantage of the proposed perturbation (of the diagonal elements of $\boldsymbol{F}(j\omega)$) is that it always adds positively to the eigenvalues of $\boldsymbol{F}(j\omega)$ and, hence, does not lead to a new passivity violation at any other frequency point. This can be proved using the following two lemmas.

Lemma 1: The real part of the frequency response of a pole is linearly proportional to the real part of its residue.

Proof of Lemma 1: For the purpose of illustration, consider the response $H_c(s)$ of a complex pole pair $-p' \pm jp''$ with the corresponding residue $r' \pm jr''$, as follows:

$$H_c(s) = \frac{r'+jr''}{s+p'-jp''} + \frac{r'-jr''}{s+p'+jp''}. \tag{22}$$

Separating (22) into real $(R(s))$ and imaginary $(I(s))$ parts, we get

$$H_c(s) = \underbrace{\frac{2r'p'(p'^2+p''^2+\omega^2) - 2r''p''(p'^2+p''^2-\omega^2)}{(p'^2+p''^2-\omega^2)^2+4p'^2\omega^2}}_{\text{Real Part }(R(s))} + j\underbrace{\frac{(r'p'-r''p'')(-4p'\omega)+2r'\omega(p'^2+p''^2-\omega^2)}{(p'^2+p''^2-\omega^2)^2+4p'^2\omega^2}}_{\text{Imaginary Part }(I(s))}. \tag{23}$$

$$\Delta\boldsymbol{C} = \begin{bmatrix} 0 & \ldots & 0 & \underset{\substack{\text{column}\\ 2m(l-1)+1\\ \downarrow}}{\Delta r_{11}^l} & 0 & \ldots & 0 & 0 & \ldots & 0 & 0 & 0 & \ldots & 0\\ & & & 0 & \Delta r_{22}^l & 0 & \vdots & & & & 0 & 0 & \ldots & 0\\ \vdots & & \vdots & & & & & \vdots & & \vdots & & & & \\ & & & \vdots & & \ddots & 0 & & & & \vdots & \vdots & & \vdots\\ 0 & & 0 & 0 & \ldots & 0 & \Delta r_{mm}^l & 0 & \ldots & 0 & 0 & 0 & \ldots & 0 \end{bmatrix}_{m\times 2mn} \tag{21}$$

From (23), it is evident that the real part of the response of a complex pole is linearly proportional to the real part of its residue. Similarly, it can be easily shown that the above is true for the case of real poles as well.

Lemma 2: If the real part of an m-port symmetric admittance matrix (represented by $\boldsymbol{F}(j\omega)$) is perturbed by a diagonal matrix $\Delta\boldsymbol{F}$, where

$$\Delta\boldsymbol{F} = \begin{bmatrix} \Delta\boldsymbol{F}_{11}(\omega) & & & \\ & \Delta\boldsymbol{F}_{22}(\omega) & & \\ & & \ddots & \\ & & & \Delta\boldsymbol{F}_{mm}(\omega) \end{bmatrix},$$
$$\Delta\boldsymbol{F}_{11}(\omega), \ldots \Delta\boldsymbol{F}_{mm}(\omega) > 0, \qquad (\omega \in \Re \cup \infty) \quad (24)$$

then the contribution of this perturbation to the eigenvalues of the $\boldsymbol{F}(j\omega)$ is nonnegative throughout the frequency spectrum.

Proof of Lemma 2: Let $\boldsymbol{y}$ and $\boldsymbol{x}$ be the left and right eigenvectors of $\boldsymbol{F}(j\omega)$. Using the eigenvalue perturbation formulas [34], we can write the contribution of (24) to an eigenvalue of $\boldsymbol{F}(j\omega)$ as

$$\Delta\lambda = \frac{\boldsymbol{y}^t \Delta\boldsymbol{F} x}{\boldsymbol{y}^t \boldsymbol{x}}, \quad \boldsymbol{x} = [x_1, \ldots x_m], \quad \boldsymbol{y} = [y_1, \ldots y_m]. \quad (25)$$

Noting that $\boldsymbol{F}(j\omega)$ is a real symmetric matrix and the fact that the left eigenvector $\boldsymbol{y}$ is equal to the right eigenvector $\boldsymbol{x}$ for a real symmetric matrix, we can write (25) as

$$\Delta\lambda = \frac{\Delta\boldsymbol{F}_{11}(\omega)x_1^2 + \Delta\boldsymbol{F}_{22}(\omega)x_2^2 + \ldots + \Delta\boldsymbol{F}_{mm}(\omega)x_m^2}{x_1^2 + x_2^2 + \ldots + x_m^2.} \quad (26)$$

It is evident from (26) that the contribution of the proposed perturbation (of the diagonal elements of $\boldsymbol{F}(j\omega)$) always adds positively to the eigenvalues of $\boldsymbol{F}(j\omega)$ and, hence, does not lead to the passivity violation at any other frequency point.

2) Error Estimation: As a result of perturbation of the residue matrix $\boldsymbol{C}$ for compensation, there will be some error introduced in the time- and frequency-domain responses. An estimation of this error can be obtained as follows.

Expressing the L_2 norm [35] of $\Delta\boldsymbol{Y}(j\omega)$, we have

$$\|\Delta\boldsymbol{Y}\|_2^2 = \int_{-\infty}^{\infty} \|\Delta\boldsymbol{Y}(j\omega)\|_F^2 \, d\omega = \int_{-\infty}^{\infty} \sum_{i=1}^{m}\sum_{j=1}^{m} |\Delta\boldsymbol{Y}_{ij}(\omega)|^2 \, d\omega$$
$$= \int_{-\infty}^{\infty} \sum_{i=1}^{m}\sum_{j=1}^{m} |\Delta\boldsymbol{Y}_{ij}(t)|^2 \, dt$$
$$= \text{trace}(\Delta\boldsymbol{C}\,\boldsymbol{P}\,\Delta\boldsymbol{C}^t) \quad (27)$$

where $\|\Delta\boldsymbol{Y}(j\omega)\|_F$ is the Frobenius norm of $\Delta\boldsymbol{Y}(j\omega)$, m is the number of ports, and $\boldsymbol{P}$ is the controllability Grammian obtained by solving the following Lyapunov equation:

$$\boldsymbol{A}\boldsymbol{P} + \boldsymbol{P}\boldsymbol{A}^t + \boldsymbol{B}\boldsymbol{B}^t = \boldsymbol{0}. \quad (28)$$

By leaving the matrices $\boldsymbol{A}$ and $\boldsymbol{B}$ unchanged and with matrix $\boldsymbol{P}$ being constant, it is evident from (27) that keeping $\|\Delta\boldsymbol{C}\| \ll \|\boldsymbol{C}\|$ will keep the error in the time and frequency domain to the minimum.

One of the major advantages of the proposed algorithm compared with the recent technique in [20] is that it provides a guaranteed search direction during passivity enforcement (i.e., passivity enforcement at one region does not lead to passivity violation at other region), thereby enabling faster convergence. Also the proposed algorithm provides additional computational advantages compared with [20], where to determine the passivity violation region as well as to enforce the passivity via perturbation of eigenvalues of the Hamiltonian matrix, the eigenvectors of the Hamiltonian matrix, which is of size $(2 \times \text{Num\_of\_Ports} \times \text{Num\_of\_Poles})$, were used. On the other hand, the proposed algorithm accomplishes the above using the eigenvectors of the transfer-function matrix, which is of size (Num_of_Ports $\times$ Num_of_Ports), much smaller than that of the Hamiltonian matrix and, hence, leads to additional CPU savings in each iteration.

A summary of the steps involved in the proposed passivity enforcement algorithm is given hereafter in the form of pseudocode.

3) Pseudocode for the Proposed Passivity Compensation Algorithm:

Step 1: Obtain multiport tabulated data up to $f_{\max}$ (maximum frequency of interest).
Step 2: Compute the multiport pole-residue model (1). Obtain the state-space system ($\boldsymbol{A}$, $\boldsymbol{B}$, $\boldsymbol{C}$, $\boldsymbol{D}$) (2).
Step 3: Construct the Hamiltonian matrix and check its eigenvalue (5).
if no imaginary eigenvalues are found, macromodel is passive. Go to **End**
else a) Determine the singular locations of $\boldsymbol{F}(j\omega)$ using Theorem 2 and collect them in a vector $\boldsymbol{S_a} = [\omega_1, \omega_2 \ldots \omega_T]$ such that $\omega_1 < \omega_2 < \ldots < \omega_T$, where "T" is the total number of such entries. Let $\omega_H = \omega_T$.
b) Determine the regions of violation using the following steps as outlined in Section IV-A:
(i) At the frequency corresponding to each of the entries in the vector $\boldsymbol{S_a}$, evaluate the slope of the eigenvalue of $\boldsymbol{F}(j\omega)$ using (12).
(ii) Count the number of positive and negative slopes starting from ω_H. When the count of positive and negative slopes become equal, say at ω_k, then the first region of local passivity violation is established (i.e., the region between ω_H to ω_k).
(iii) Reset the count of slope to zero and designate $\omega_H = \omega_{k-1}$

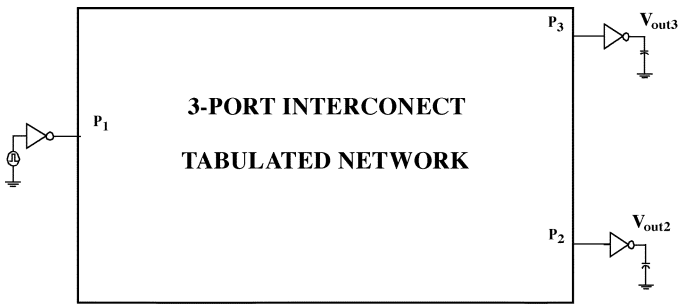

Fig. 3. Three-port interconnect network.

and repeat steps (ii) and (iii) until all entries in the set S_a are exhausted.

c) Determine the exact location of maximum passivity violation in every region of violation using (13).

d) Identify the poles used for compensation using (17) and then select the corresponding residues of driving point admittances (as per the guidelines in Section IV-C) and formulate ΔC.

e) Perform the passivity compensation by computing ΔC at each point of maximum violation determined in c) using (16). Go to **End**

End

V. Computational Results

In this section, two examples are presented to demonstrate the efficiency and accuracy of the proposed compensation algorithm.

Example 1: Three-Port Tabulated Data: In this example, the proposed compensation algorithm was performed on the tabulated data obtained from a three-port interconnect subnetwork [3] (Fig. 3). The subnetwork was characterized by a set of tabulated data (Y -parameters) up to 6 GHz (henceforth referred to as the *original data*). The data was fitted using the algorithm described in [5] (40 complex poles and four real poles were required; all were stable poles and are listed in Table I) and the state–space macromodel was obtained. The macromodel is tested for passivity using Theorem 1 of Section III by solving the Hamiltonian matrix (5). In this case, six imaginary eigenvalues were found, indicating that the macromodel is nonpassive. The details of the eigenvalue spectrum of the Hamiltonian matrix are given in Fig. 4(a). For the purpose of clarity, Fig. 4(b) shows an enlarged view of the eigenvalue spread near the imaginary axis and also shows the exact numerical values of the imaginary eigenvalues. According to Theorem 2 of Section III, these imaginary eigenvalues correspond to the exact locations at which eigenvalues of Real$(\boldsymbol{Y}(j\omega))$ become zero. Fig. 5 confirms this result, which shows the eigenvalue spectrum of Real$(\boldsymbol{Y}(j\omega))$.

TABLE I
List of Poles for Example 1

Poles for Example 1
-9.3844e-002 ± 3.8276e+001i
-1.5689e-001 ± 3.6162e+001i
-2.9388e-001 ± 3.4761e+001i
-6.8818e-002 ± 3.2396e+001i
-9.5903e-002 ± 3.1124e+001i
-1.8371e-001 ± 2.8294e+001i
-1.6891e-001 ± 2.8017e+001i
-1.5723e-001 ± 2.4263e+001i
-2.9318e-001 ± 2.3702e+001i
-1.2720e-001 ± 2.1614e+001i
-3.1590e-001 ± 1.9997e+001i
-6.3208e-001 ± 1.8482e+001i
-2.2797e-001 ± 1.5844e+001i
-2.6499e-001 ± 1.3414e+001i
-3.7967e-001 ± 1.2015e+001i
-3.2720e-001 ± 9.1904e+000i
-3.6646e-001 ± 7.7105e+000i
-1.1781e+000 ± 6.7644e+000i
-8.8563e-001 ± 5.3921e+000i
-1.3786e+000 ± 3.5099e+000i
-1.2995e+000
-1.1772e-001
-8.4539e-002
-1.3593e-001

As seen in this figure, Real$(\boldsymbol{Y}(j\omega))$ becomes singular at six frequency points, exactly corresponding to the imaginary eigenvalues of the Hamiltonian matrix.

The regions of passivity violation were then determined using the method in Section IV-A. In this example, three regions of passivity violation were found, and they are indicated in both Figs. 5 and 6. In each region, the location of maximum passivity violation was determined using (13) of Section IV-B, and the corresponding details are given in Table II.

With the above information of exact locations of passivity violation, passivity correction was performed using the steps proposed in Section IV-C by perturbing the selected residues of diagonal elements of the admittance matrix. The details of poles and selected residues (before and after perturbation) and the relative norm of the perturbed residue matrix ($||\Delta C||$) are summarized in Table II.

Fig. 6 shows the eigenvalue spectrum of Real$(\boldsymbol{Y}(j\omega))$ before and after the compensation. As indicated by the dotted line, all violations were corrected by the proposed algorithm. This is also

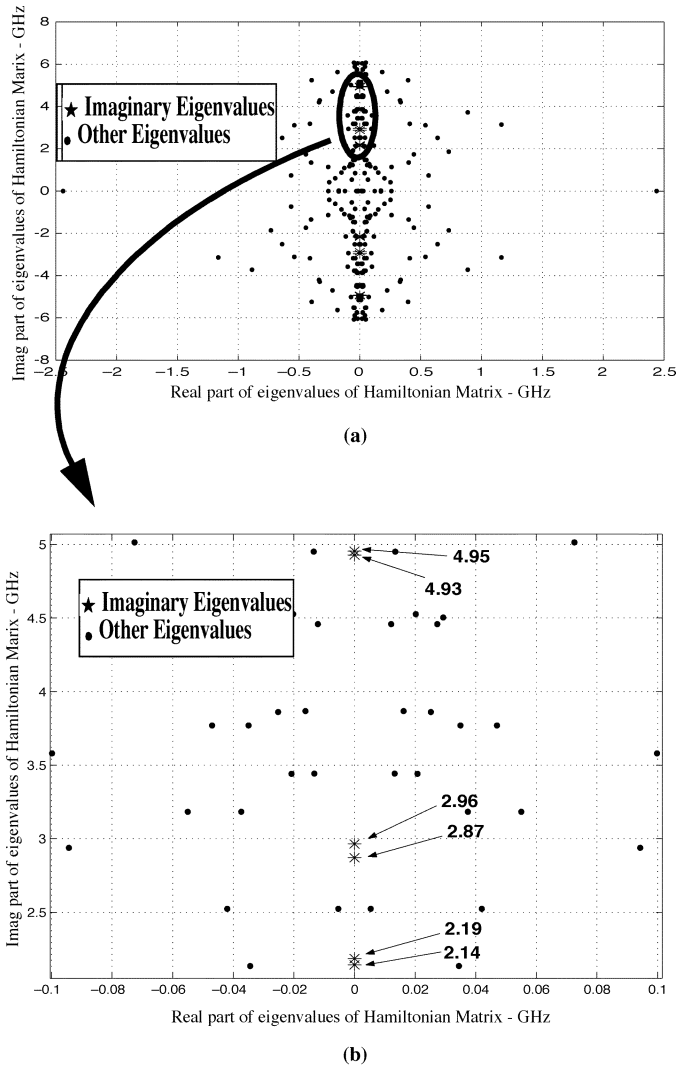

Fig. 4. (a) Eigenvalue spectrum of Hamiltonian matrix (example 1). (b) Enlarged view of eigenvalue spectrum.

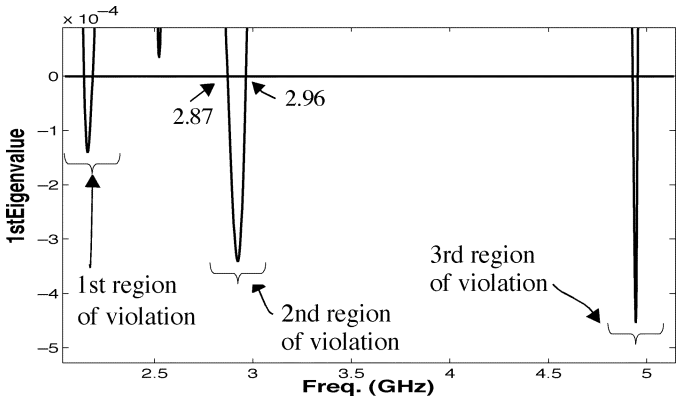

Fig. 5. Eigenvalue versus frequency of Real($\boldsymbol{Y}(j\omega)$)—(example 1).

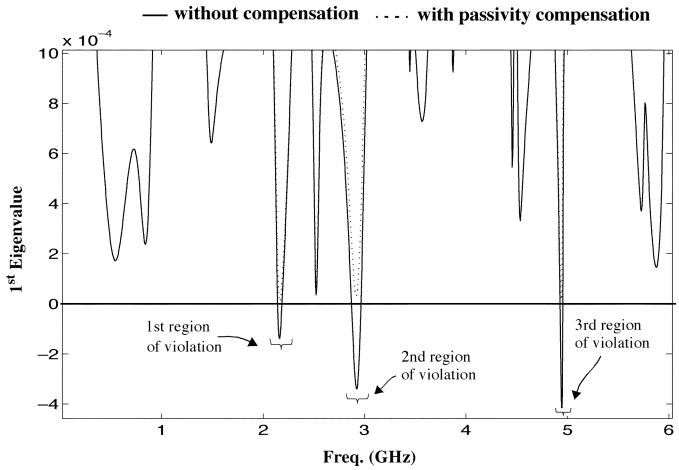

Fig. 6. Eigenvalue versus frequency of Real($\boldsymbol{Y}(j\omega)$)—with proposed passivity compensation.

verified by formulating the Hamiltonian matrix (5) of the compensated macromodel. Figs. 7 and 8 show the comparison between the original data and the response of the proposed passive macromodel, and they match accurately. The MATLAB implementation of the proposed algorithm on a Sun-Blade-100 machine required 6.49 s.

Next, the passive macromodel is linked to HSPICE and a nonlinear transient analysis is performed for an input pulse having a rise and fall time of 0.1 ns and pulsewidth of 5 ns. The result at node $\mathbf{P_1}$ is shown in Fig. 9. For validation purposes, the original network (from which the tabulated data was obtained) was also subjected to the transient analysis (using HSPICE) with similar input and terminations, and the results are compared in Fig. 9. As seen, both match accurately.

It is to be noted that, while using the proposed global passivity enforcement algorithm, no additional regions of passivity violation were introduced during the compensation process (since it employs a guaranteed search direction for enforcing passivity). On the other hand, for comparison purposes, when the passivity compensation algorithms of [17] and [21] are used, two new passivity violation regions were introduced while performing the compensation at the above three regions. It is to be noted that this problem could be aggravated in the presence of many regions of passivity violations in the original macromodel and also for macromodels with a large number of ports.

Example 2: Four-Port Tabulated Data: In this example, the proposed algorithm was performed on the tabulated $\boldsymbol{Y}$ parameters of a four-port interconnect subnetwork (Fig. 10). The data was fitted using the algorithm described in [5] (20 complex poles and four real poles were required; all were stable poles), and the state–space macromodel was obtained. The macromodel is tested for passivity using Theorem 1 of Section III by solving the Hamiltonian matrix (5). In this case, two imaginary eigenvalues were found, indicating that the macromodel is nonpassive. This is confirmed by the corresponding eigenvalue spectrum of Real($\boldsymbol{Y}(j\omega)$), which is given in Fig. 11(a).

The regions of passivity violation were then determined using the method in Section IV-A. In this example, one region of passivity violation was found and is indicated in Fig. 11(a). In this region of violation, the location of maximum passivity violation was determined using (13) of Section IV-B, and the corresponding details are given in Table III.

With this information of exact location of passivity violation, passivity correction was performed using the algorithm proposed in Section IV-C by perturbing the selected residues of diagonal

TABLE II
DETAILS OF PROPOSED PASSIVITY CORRECTION ALGORITHM FOR EXAMPLE 1

	Region of Violation No.1	**Region of Violation** No.2	**Region of Violation** No.3
f_l	4.93 GHz	2.87 GHz	2.14 GHz
f_h	4.95 GHz	2.96 GHz	2.19 GHz
Location of Maximum Violation	4.9449 GHz	2.9230 GHz	2.1605 GHz
Maximum Violation (Eigenvalue of $F(j\omega)$)	-4.5944e-4	-3.4105e-4	-1.4078e-4
Poles Considered during Compensation	-6.8818e-2 ± 3.2396e+1i -9.5903e-2 ± 3.1124e+1i -1.8371e-1 ± 2.8294e+1i	-3.1590e-1 ± 1.9997e+1i -6.3208e-1 ± 1.8482e+1i -2.2797e-1 ± 1.5844e+1i	-2.6499e-1 ± 1.3414e+1i -3.7967e-1 ± 1.2015e+1i
Residues Prior to Compensation			
Y_{11}	4.8169e-4 ± 7.6047e-6i 9.3618e-3 ± 1.5375e-4i 1.3849e-2 ± 1.1482e-3i	3.6197e-3 ± 2.8452e-4i 2.5574e-2 ± 1.0757e-3i 4.3985e-3 ± 9.5013e-4i	2.5452e-3 ± 2.2433e-3i 2.6578e-3 ± 2.6693e-4i
Y_{22}	2.8498e-4 ± 3.5028e-6i 6.9539e-2 ± 4.3490e-3i 2.9437e-2 ± 1.6749e-3i	9.8733e-4 ± 3.2117e-4i 1.5195e-2 ± 3.8187e-3i 3.6676e-4 ± 6.9578e-4i	7.2920e-2 ± 7.3045e-3i 3.6715e-4 ± 1.9476e-4i
Y_{33}	4.3613e-2 ± 4.1242e-3i 2.0500e-4 ± 1.5760e-4i 1.8595e-2 ± 3.8426e-4i	5.1665e-2 ± 8.7504e-3i -1.6837e-4 ± 2.7814e-4i 4.6962e-2 ± 7.1124e-3i	-6.3402e-5 ± 4.6018e-4i 2.8735e-2 ± 7.8639e-3i
Residues after Compensation			
Y_{11}	4.8169e-4 ± 7.6047e-6i 9.3631e-3 ± 1.5375e-4i 1.3849e-2 ± 1.1482e-3i	3.6343e-3 ± 2.8452e-4i 2.5769e-2 ± 1.0757e-3i 4.4031e-3 ± 9.5013e-4i	2.5506e-3 ± 2.2433e-3i 2.6580e-3 ± 2.6693e-4i
Y_{22}	2.8498e-4 ± 3.5028e-6i 6.9539e-2 ± 4.3490e-3i 2.9437e-2 ± 1.6749e-3i	1.0082e-3 ± 3.2117e-4i 1.5475e-2 ± 3.8187e-3i 3.7328e-4 ± 6.9578e-4i	7.2920e-2 ± 7.3045e-3i 3.6717e-4 ± 1.9476e-4i
Y_{33}	4.3614e-2 ± 4.1242e-3i 2.7017e-4 ± 1.5760e-4i 1.8595e-2 ± 3.8426e-4i	5.1666e-2 ± 8.7504e-3i -1.6623e-4 ± 2.7814e-4i 4.6963e-2 ± 7.1124e-3i	-2.7867e-6 ± 4.6018e-4i 2.8739e-2 ± 7.8639e-3i
$\frac{\|\Delta C\|}{\|C\|}$	3.3888e-4	1.4198e-3	1.419801e-3

elements of the admittance matrix. Due to the guaranteed search direction for enforcing passivity used in the algorithm, no additional regions of passivity violation were introduced during compensation. The details of the poles whose residues are perturbed and the relative norm of the perturbed residue matrix $||\Delta \boldsymbol{C}||$ are summarized in the Table III.

Fig. 11(b) shows the eigenvalue spectrum of Real$(\boldsymbol{Y}(j\omega))$ before and after the compensation. Figs. 12 and 13 show a sample of comparisons between the original data and the response of the proposed passive macromodel, and they match accurately. Next, a nonlinear transient analysis is performed by replacing the four-port linear network in Fig. 10 with the proposed macromodel for an input pulse having a rise and fall time of 0.1 ns and pulsewidth of 5 ns (using HSPICE). For validation purposes, the original network from which the data was obtained was also subjected to the transient analysis (using HSPICE) with the similar input and terminations, and the corresponding transient results are compared in Fig. 14. As seen, both match accurately.

VI. CONCLUSION

In this paper, an algorithm has been presented for passivity compensation of nonpassive macromodels obtained from

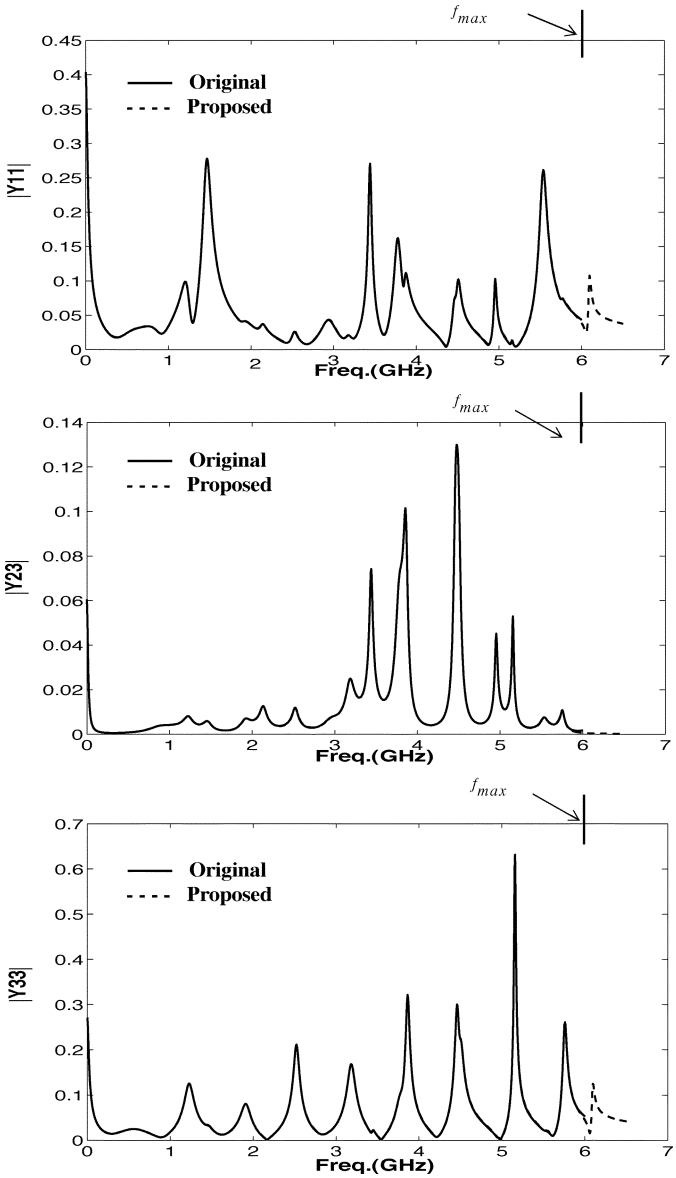

Fig. 7. Frequency responses (magnitude) for example 1.

tabulated data. The algorithm presented here is based on a guaranteed search direction for passivity correction and performs compensation without introducing any new regions of passivity violation. This overcomes the major limitation of local passivity enforcing algorithms in literature, which are prone to introduce new regions of passivity violation during the passivity compensation process. The paper also provides an error estimate for the response of the passivity-compensated macromodel. Numerical examples are presented to validate the validity and accuracy of the proposed algorithm.

APPENDIX A

In this appendix, we show the proof of the corollary of Theorem 2: "the Hamiltonian matrix $\boldsymbol{M}$ has an eigenvalue $j\omega_0$, if the real part of the corresponding symmetric admittance matrix, $\boldsymbol{F}(j\omega_0)$ is singular, provided $\boldsymbol{D}+\boldsymbol{D}^t$ is a positive definite matrix."

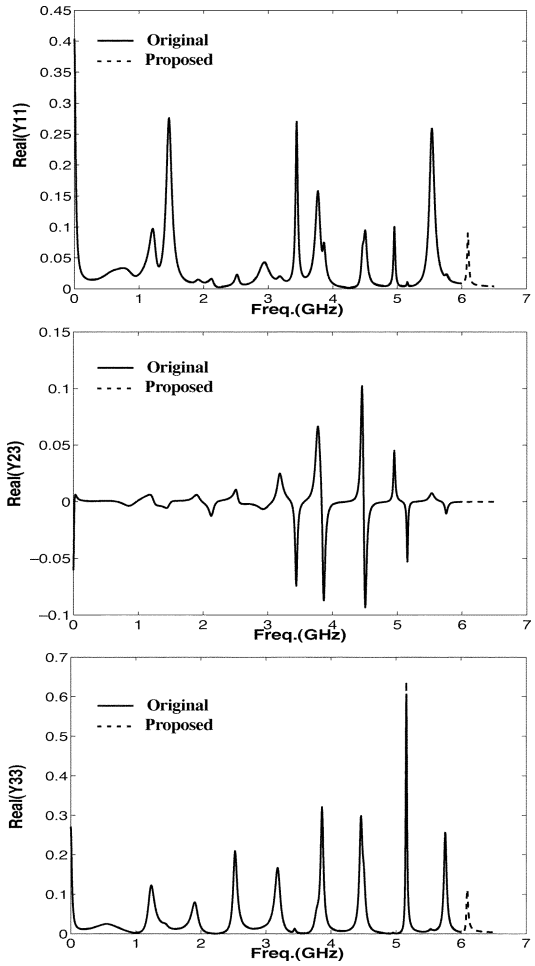

Fig. 8. Frequency responses (real part) for example 1.

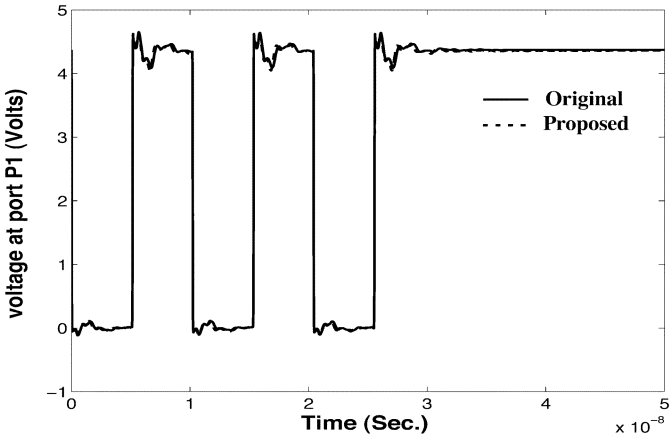

Fig. 9. Transient result of example 1.

Let us start by assuming that $\boldsymbol{F}(j\omega)$ is singular at frequency ω_0. This means that $\boldsymbol{F}(j\omega_0)$ has an eigenvalue that is zero, i.e.,

$$\boldsymbol{F}(j\omega_0)\boldsymbol{u} = 0\boldsymbol{u} \tag{29}$$

or

$$\boldsymbol{F}(j\omega_0)\boldsymbol{u} = \boldsymbol{0} \tag{30}$$

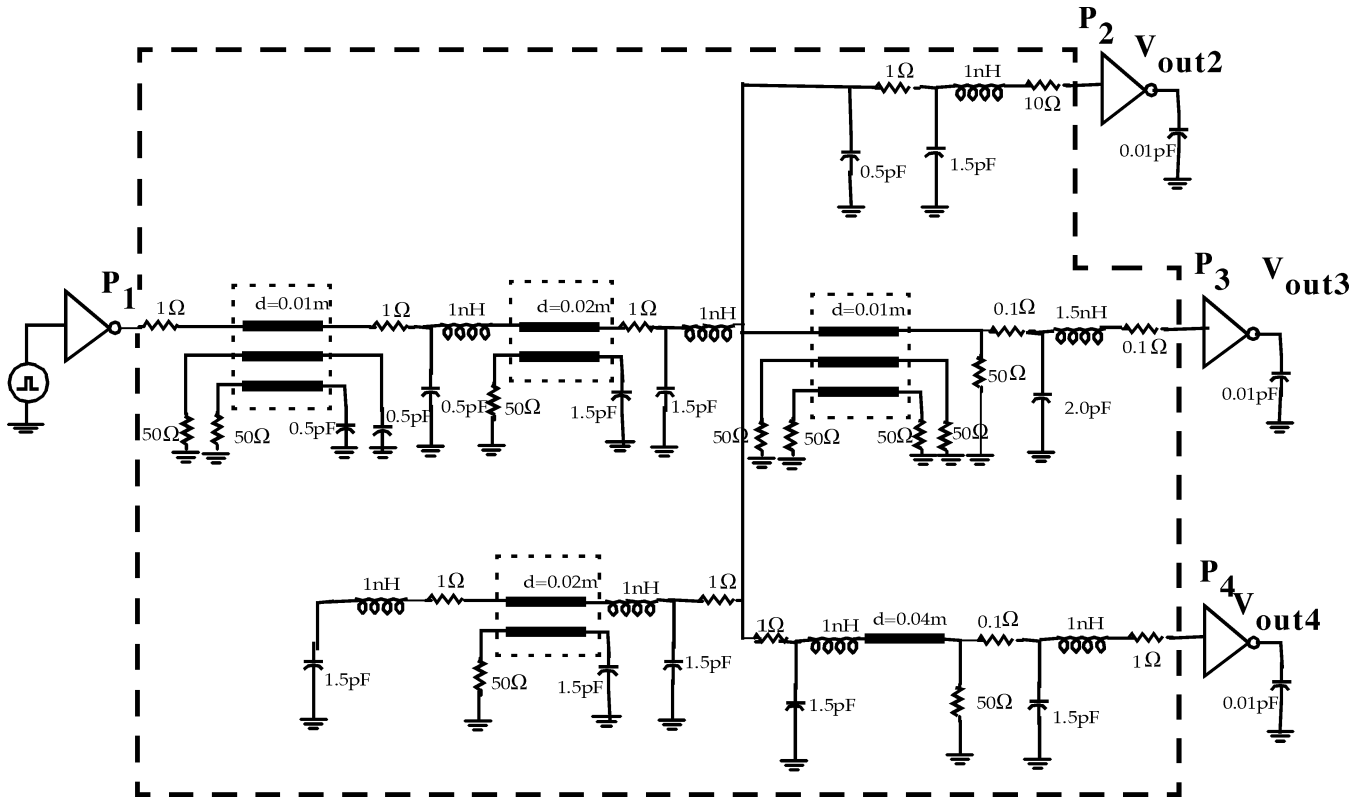

Fig. 10. Four-port interconnect subnetwork (example 2).

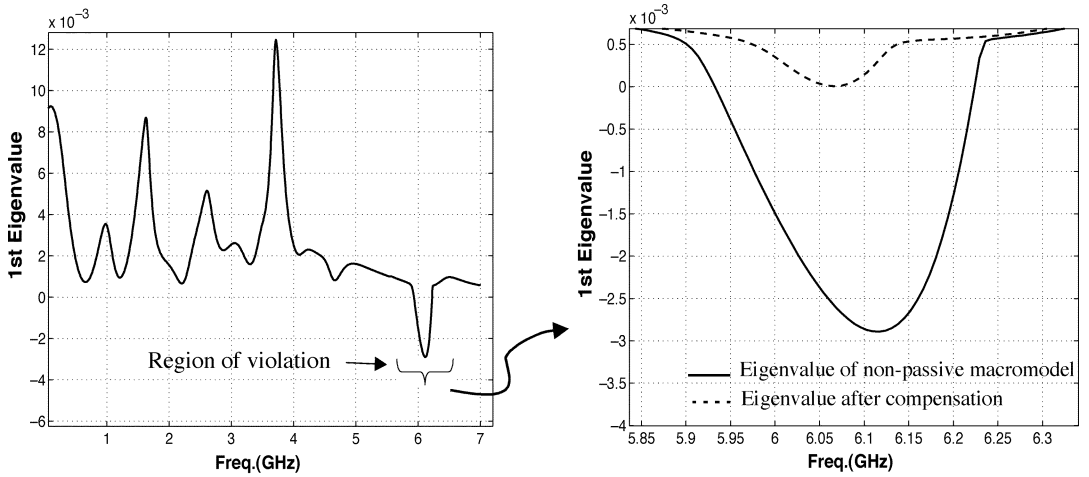

(a) (b)

Fig. 11. Eigenvalues of Real($\boldsymbol{Y}(j\omega)$) for example 2. (a) Nonpassive macromodel. (b) Enlarged view: Comparison of eigenvalues of nonpassive and compensated macromodels.

where $\boldsymbol{u}$ is the eigenvector in the null space of $\bar{\boldsymbol{F}}(j\omega_0)$. Noting that $\boldsymbol{F}(j\omega_0) = [\boldsymbol{Y}^t(j\omega_0^*) + \boldsymbol{Y}(j\omega_0)]/2$ and using (3), (30) can be rewritten as

$$\left(\boldsymbol{C}(j\omega_0\boldsymbol{I}-\boldsymbol{A})^{-1}\boldsymbol{B}+\boldsymbol{D}+\boldsymbol{B}^t(-j\omega_0\boldsymbol{I}-\boldsymbol{A}^t)^{-1}\boldsymbol{C}^t+\boldsymbol{D}^t\right)\boldsymbol{u}=\boldsymbol{0} \tag{31}$$

or

$$\boldsymbol{C}(j\omega_0\boldsymbol{I}-\boldsymbol{A})^{-1}\boldsymbol{B}\boldsymbol{u}+\boldsymbol{B}^t(-j\omega_0\boldsymbol{I}-\boldsymbol{A}^t)^{-1}\boldsymbol{C}^t\boldsymbol{u} = -(\boldsymbol{D}+\boldsymbol{D}^t)\boldsymbol{u}. \tag{32}$$

Substituting

$$-(j\omega_0\boldsymbol{I}-\boldsymbol{A})^{-1}\boldsymbol{B}\boldsymbol{u} = \boldsymbol{r} \tag{33}$$

and

$$(-j\omega_0\boldsymbol{I}-\boldsymbol{A}^t)^{-1}\boldsymbol{C}^t\boldsymbol{u} = \boldsymbol{s} \tag{34}$$

we can write (32) as

$$-\boldsymbol{C}\boldsymbol{r}+\boldsymbol{B}^t\boldsymbol{s} = -(\boldsymbol{D}+\boldsymbol{D}^t)\boldsymbol{u} \tag{35}$$

or

$$[-\boldsymbol{C}\ \boldsymbol{B}^t]\begin{bmatrix}\boldsymbol{r}\\ \boldsymbol{s}\end{bmatrix} = -(\boldsymbol{D}+\boldsymbol{D}^t)\boldsymbol{u} \tag{36}$$

TABLE III
DETAILS OF PROPOSED PASSIVITY CORRECTION ALGORITHM FOR EXAMPLE 2

	Region of Violation No.1
f_l	5.9327 GHz
f_h	6.2238 GHz
Location of Maximum Violation	6.115 GHz
Maximum Violation (Eigenvalue of $F(j\omega)$)	-2.8923e-3
Poles Considered during Compensation	-1.3150 ± 4.0243e+1i -2.4110e-1 ± 3.4912e+1i
Residues Prior to Compensation	
Y_{11}	2.4078e-002 ± 6.2584e-002i 8.3741e-002 ± 9.1161e-004i
Y_{22}	1.1441e-003 ± 1.7809e-003i 3.0684e-003 ± 2.5928e-003i
Y_{33}	3.8586e-004 ± 7.0019e-004i 2.4401e-004 ± 1.7869e-004i
Y_{44}	2.5653e-003 ± 3.8721e-003i 3.3408e-004 ± 2.9410e-004i
Residues after Compensation	
Y_{11}	3.6665e-002 ± 6.2584e-002i 8.4695e-002 ± 9.1161e-004i
Y_{22}	1.2194e-003 ± 1.7809e-003i 3.0741e-003 ± 2.5928e-003i
Y_{33}	4.4661e-004 ± 7.0019e-004i 2.4953e-004 ± 1.7869e-004i
Y_{44}	2.5805e-003 ± 3.8721e-003i 3.3528e-004 ± 2.9410e-004i
$\frac{\|\Delta C\|}{\|C\|}$	1.39e-2

or

$$-(\boldsymbol{D}+\boldsymbol{D}^t)^{-1}[-\boldsymbol{C}\,\boldsymbol{B}^t]\begin{bmatrix}\boldsymbol{r}\\ \boldsymbol{s}\end{bmatrix}=\boldsymbol{u}. \tag{37}$$

Next, using (33) and (34), we get

$$-\boldsymbol{B}\boldsymbol{u}=(j\omega_0\boldsymbol{I}-\boldsymbol{A})\boldsymbol{r} \tag{38}$$

and

$$-\boldsymbol{C}^t\boldsymbol{u}=(j\omega_0\boldsymbol{I}+\boldsymbol{A}^t)\boldsymbol{s} \tag{39}$$

respectively. Combining (38) and (39), we get

$$\begin{bmatrix}-\boldsymbol{B}\\ -\boldsymbol{C}^t\end{bmatrix}\boldsymbol{u}=\begin{bmatrix}(j\omega_0\boldsymbol{I}-\boldsymbol{A}) & \\ & (j\omega_0\boldsymbol{I}+\boldsymbol{A}^t)\end{bmatrix}\begin{bmatrix}\boldsymbol{r}\\ \boldsymbol{s}\end{bmatrix}. \tag{40}$$

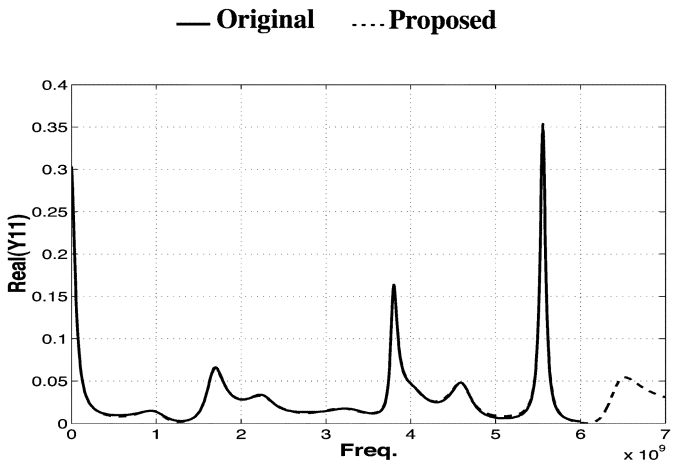

Fig. 12. Sample admittance parameter for example 2—real part.

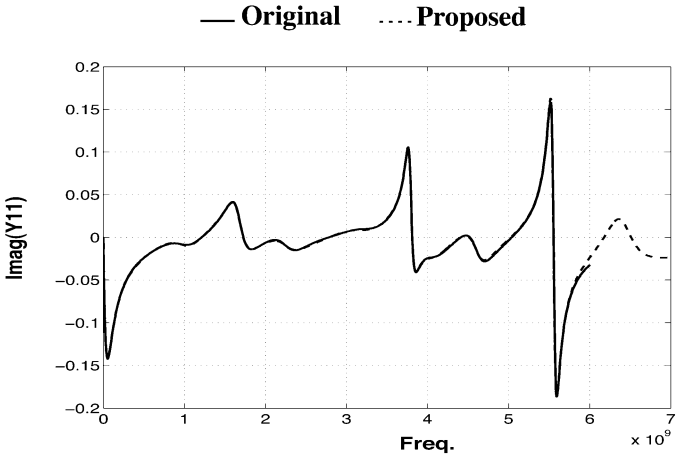

Fig. 13. Sample admittance parameter for example 2—imaginary part.

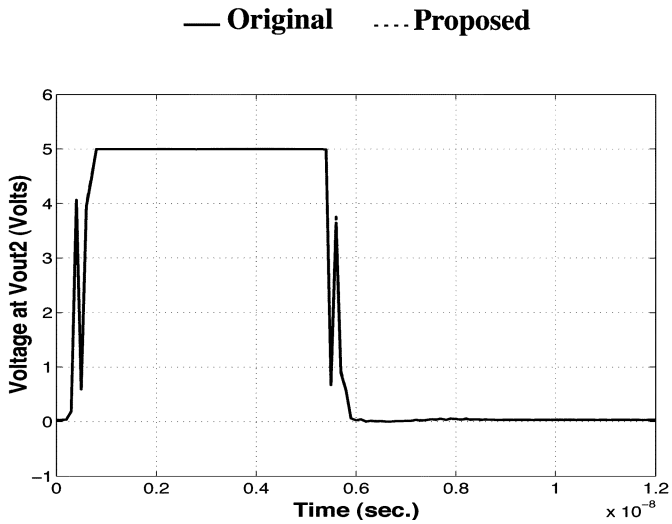

Fig. 14. Transient response (example 2).

Now, substituting $\boldsymbol{u}$ from (37) in (40), we get

$$\begin{bmatrix}\boldsymbol{B}\\ \boldsymbol{C}^t\end{bmatrix}(\boldsymbol{D}+\boldsymbol{D}^t)^{-1}[-\boldsymbol{C}\,\boldsymbol{B}^t]\begin{bmatrix}\boldsymbol{r}\\ \boldsymbol{s}\end{bmatrix}=\begin{bmatrix}(j\omega_0\boldsymbol{I}-\boldsymbol{A}) & \\ & (j\omega_0\boldsymbol{I}+\boldsymbol{A}^t)\end{bmatrix}\begin{bmatrix}\boldsymbol{r}\\ \boldsymbol{s}\end{bmatrix} \tag{41}$$

or

$$\begin{bmatrix} -\boldsymbol{B}(\boldsymbol{D}+\boldsymbol{D}^t)^{-1}\boldsymbol{C} & \boldsymbol{B}(\boldsymbol{D}+\boldsymbol{D}^t)^{-1}\boldsymbol{B}^t \\ -\boldsymbol{C}^t(\boldsymbol{D}+\boldsymbol{D}^t)^{-1}\boldsymbol{C} & \boldsymbol{C}^t(\boldsymbol{D}+\boldsymbol{D}^t)^{-1}\boldsymbol{B}^t \end{bmatrix} \begin{bmatrix} \boldsymbol{r} \\ \boldsymbol{s} \end{bmatrix} = j\omega_0 \begin{bmatrix} \boldsymbol{r} \\ \boldsymbol{s} \end{bmatrix} + \begin{bmatrix} -\boldsymbol{A} & \\ & \boldsymbol{A}^t \end{bmatrix} \begin{bmatrix} \boldsymbol{r} \\ \boldsymbol{s} \end{bmatrix} \quad (42)$$

or

$$\begin{bmatrix} \boldsymbol{A}-\boldsymbol{B}(\boldsymbol{D}+\boldsymbol{D}^t)^{-1}\boldsymbol{C} & \boldsymbol{B}(\boldsymbol{D}+\boldsymbol{D}^t)^{-1}\boldsymbol{B}^t \\ -\boldsymbol{C}^t(\boldsymbol{D}+\boldsymbol{D}^t)^{-1}\boldsymbol{C} & -\boldsymbol{A}^t+\boldsymbol{C}^t(\boldsymbol{D}+\boldsymbol{D}^t)^{-1}\boldsymbol{B}^t \end{bmatrix} \begin{bmatrix} \boldsymbol{r} \\ \boldsymbol{s} \end{bmatrix} = j\omega_0 \begin{bmatrix} \boldsymbol{r} \\ \boldsymbol{s} \end{bmatrix}. \quad (43)$$

Noting that the Hamiltonian matrix $\boldsymbol{M}$ is defined as in (5), we can write (43) as

$$\boldsymbol{M} \begin{bmatrix} \boldsymbol{r} \\ \boldsymbol{s} \end{bmatrix} = j\omega_0 \begin{bmatrix} \boldsymbol{r} \\ \boldsymbol{s} \end{bmatrix}. \quad (44)$$

It is evident from (44) that $j\omega_0$ is the eigenvalue of Hamiltonian matrix $\boldsymbol{M}$ as defined in (5). Next, correlating this information with the initial assumption we started with, i.e., $\boldsymbol{F}(j\omega)$ is singular at frequency ω_0, we can infer that the frequency point at which $\boldsymbol{F}(j\omega)$ is singular corresponds to the imaginary eigenvalue of the Hamiltonian matrix $\boldsymbol{M}$.

REFERENCES

[1] W. T. Beyene and J. E. Schutt-Aine, "Accurate frequency-domain modeling and simulation of high-speed packaging interconnects," *IEEE Trans. Microw. Theory Tech.*, vol. 45, no. 10, pp. 1941–1947, Oct. 1997.

[2] M. Elzinga, K. L. Virga, L. Zhao, and J. L. Prince, "Pole-residue formulation for transient simulation of high-frequency interconnects using householder LS curve-fitting techniques," *IEEE Trans. Adv. Packag.*, vol. 25, no. 2, pp. 142–147, May 2000.

[3] R. Achar, P. Gunupudi, M. Nakhla, and E. Chiprout, "Passive interconnect reduction algorithm for distributed/measured networks," *IEEE Trans. Circuits Syst. II. Analog Digit. Signal Process.*, vol. 47, no. 4, pp. 287–301, Apr. 2000.

[4] D. Saraswat, R. Achar, and M. Nakhla, "Restoration of passivity in S-parameter data of microwave measurements," presented at the IEEE Int. Microwave Symp., Long Beach, CA, Jun. 12–17, 2005.

[5] B. Gustavsen and A. Semlyen, "Rational approximation of frequency domain responses by vector fitting," *IEEE Trans. Power Del.*, vol. 14, no. 2, pp. 1052–1061, Jul. 1999.

[6] D. Saraswat, R. Achar, and M. Nakhla, "A fast algorithm and practical considerations for passive macromodeling of measured/simulated data," in *Proc. IEEE 11th Topical Meeting Electrical Performance Electronic Packaging*, Monterey, CA, Oct. 2002, pp. 297–300.

[7] ——, "A fast algorithm and practical considerations for passive macromodeling of measured/simulated data," *IEEE Trans. Compon. Packag. Manufact. Technol.*, vol. 27, no. 1, pp. 57–70, Feb. 2004.

[8] W. T. Beyene and J. E. Schutt-Aine, "Efficient transient simulation of high-speed interconnects characterized by sampled data," *IEEE Trans. Compon., Packag., Manuf. Technol.*, pt. B, vol. 21, no. 1, pp. 105–114, Feb. 1998.

[9] ——, "Interconnect simulation using order reduction and scattering parameters," in *IEEE Electronic Components Tech. Conf.*, 1998, pp. 627–631.

[10] M. Elzinga, K. L. Virga, and J. L. Prince, "Improved global rational approximation macro-modeling algorithm for networks characterized by frequency-sampled data," *IEEE Trans. Microw. Theory Tech.*, vol. 48, no. 9, pp. 1461–1468, Sep. 2000.

[11] C. P. Coelho, J. R. Phillips, and L. M. Silveira, "Robust rational function approximation algorithm for model generation," in *Proc. 36th Design Automation Conf.*, New Orleans, LA, Jun. 1999, pp. 207–212.

[12] S. Min and M. Swaminathan, "Efficient construction of two port passive macromodels for resonant networks," in *IEEE 10th Topical Meeting Electrical Performance of Electronic Packaging (EPEP)*, Cambridge, MA, Oct. 2001, pp. 229–232.

[13] J. Morsey and A. C. Cangellaris, "Passive realization of interconnect models from measured data," in *IEEE 10th Topical Meeting Electrical Performance of Electronic Packaging (EPEP)*, Cambridge, MA, Oct. 2001, pp. 47–50.

[14] C. P. Coelho, J. R. Phillips, and L. M. Silveira, "Passive constrained rational approximation algorithm using nevanlinna-pick interpolation," in *Proc. 2002 Design, Automation Test Eur. Conf. Exhibition*, Mar. 2002, pp. 923–930.

[15] ——, "A convex programming approach to positive real rational approximation," in *Proc. IEEE/ACM Int. Conf. Computer Aided Design*, Nov. 2001, pp. 245–251.

[16] L. M. Silveria, I. M. Elfadel, J. K. White, M. Chilukuri, and K. S. Kundert, "An efficient approach to transmission line simulation using measured or tabulated S-parameter data," in *Proc. ACM/IEEE Design Automation Conf.*, Jun. 1994, pp. 634–639.

[17] B. Gustavsen and A. Semlyen, "Enforcing passivity for admittance matrices approximated by rational functions," *IEEE Trans. Power Syst.*, vol. 16, no. 1, pp. 97–104, Feb. 2001.

[18] R. Neumayer, F. Haslinger, A. Stelzer, and R. Weigel, "On the synthesis of equivalent circuit models for multiports characterized by frequency-dependent parameters," *IEEE Trans. Microw. Theory Tech.*, vol. 50, no. 12, pp. 2789–2796, Dec. 2002.

[19] D. Saraswat, R. Achar, and M. Nakhla, "Passive macromodels of microwave subnetworks characterized by measured/simulated data," in *Proc. Int. Microwave Symp. 2003 Dig.*, Philadelphia, PA, Jun. 2003, pp. 999–1002.

[20] S. Grivet-Talocia, "Passivity enforcement via perturbation of Hamiltonian matrices," *IEEE Trans. Circuits Syst.—I: Fundam. Theory Appl.*, vol. 51, no. 9, pp. 1755–1769, Sep. 2004.

[21] D. Saraswat, R. Achar, and M. Nakhla, "On passivity check and compensation of macro-models from tabulated data," in *Proc. 7th IEEE Workshop Signal Propagation Interconnects*, Siena, Italy, May 2003, pp. 25–28.

[22] A. Odabasioglu, M. Celik, and L. T. Pillage, "PRIMA: Passive reduced-order interconnect macromodeling algorithm," *IEEE Trans. Comput.-Aided Des. Integr. Circuits Syst.*, vol. 17, no. 8, pp. 645–654, Aug. 1998.

[23] A. Dounavis, E. Gad, R. Achar, and M. Nakhla, "Passive model-reduction of multiport distributed networks including frequency-dependent parameters," *IEEE Trans. Microw. Theory Tech.*, vol. 48, no. 12, pp. 2325–2334, Dec. 2000.

[24] R. Achar and M. Nakhla, "Simulation of high-speed interconnects," *Proc. IEEE*, vol. 89, pp. 693–728, May 2001.

[25] M. Nakhla and R. Achar, *Multimedia Book Series on Signal Integrity*. Ottawa, ON, Canada: OMNIZ Global Knowledge Corp., 2002.

[26] T. Kailath, *Linear Systems*. Englewood Cliffs, NJ: Prentice-Hall, 1980.

[27] C. T. Chen, *Linear System Theory and Design*. New York: Holt, Rinehart and Winston, 1984.

[28] R. Achar and M. Nakhla, *Minimum Realization of Reduced-Order Models of High-Speed Interconnect Macromodels, Chapter III: Signal Propagation on Interconnects*. Norwell, MA: Kluwer, 1998, pp. 23–45.

[29] E. Kuh and R. Rohrer, *Theory of Active Linear Networks*. San Francisco, CA: Holden-Day, 1967.

[30] L. Weinberg, *Network Analysis and Synthesis*. New York: McGraw-Hill, 1962.

[31] M. E. Valkenburg, *Introduction to Modern Network Synthesis*. New York: Wiley, 1960.

[32] S. Boyd, L. E. Ghaoui, E. Feron, and V. Balakrishnan, *Linear Matrix Inequalities in System and Control Theory*. Philadelphia, PA: SIAM, 1994, vol. 15.

[33] P. A. Parrilo, "Structured semidefinite programs and semialgebraic geometry methods in robustness and optimization," Ph.D. dissertation, Dept. of Control and Dynamical Systems, California Institute of Technology, Pasadena, 2000.

[34] G. W. Stewart and J. Sun, *Matrix Perturbation Theory*. Boston, MA: Academic, 1990.

[35] K. Zhou and J. C. Doyle, *Essentials of Robust Control*. Upper Saddle River, NJ: Prentice-Hall, 1998.

Dharmendra Saraswat (S'03) received the B.E. degree from Government Engineering College (GEC), Jabalpur, India, in 1990, and M.A.Sc. degree from Carleton University, Ottawa, ON, Canada, in 2003. He is currently working toward the Ph.D. degree in electrical engineering at Carleton University.

His research interests include the modeling and simulation of high-speed interconnect networks, circuit simulation, and numerical algorithms.

Mr. Saraswat received the 2002 Best Student Paper Award presented at the Electrical Performance of Electronic Packaging Conference, and the Third Best Student Paper Award presented at the International Microwave Symposium in 2003. He is also the recipient of the Natural Sciences and Engineering Research Council (NSERC) Scholarship at the doctoral level.

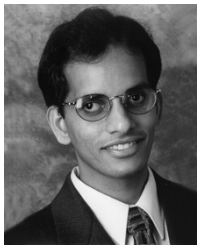

Ramachandra Achar (S'95–M'00–SM'04) received the B.Eng. degree in electronics engineering from Bangalore University, India, in 1990, the M.Eng. degree in microelectronics from Birla Institute of Technology and Science, Pilani, India, in 1992, and the Ph.D. degree from Carleton University, Ottawa, ON, Canada, in 1998.

In summer 1995, he worked on high-speed interconnect analysis at T. J. Watson Research Center, IBM, New York. He was a Research and Development Engineer at Larsen and Toubro Engineers, Ltd., Mysore, India, and at Indian Institute of Science, Bangalore, India. In 1992, he was a graduate trainee at Central Electronics Engineering Research Institute, Pilani, India. From 1998 to 2000, he served as a Research Engineer in the Compter-Aided Engineering (CAE) group at Carleton University, where he currently serves as an Assistant Professor in the Department of Electronics. He is a also a Consultant for several leading industries focused on high-frequency circuits, systems, and tools. He has published more than 100 peer-reviewed articles in international journals/conferences, six multimedia books on signal integrity, and four chapters in different books. His research interests include signal integrity analysis, numerical algorithms and development of computer-aided design tools for modeling and simulation of high-frequency interconnects, nonlinear circuits, microwave/radio-frequency networks, optoelectronic devices, microelectromechanical systems (MEMS), and electromagnetic compatibility/electromagnetic interference.

Dr. Achar received several prestigious awards, including the University Medal for outstanding doctoral work (1998), the Natural Science and Engineering Research Council (NSERC) doctoral medal (2000), the Strategic Microelectronics Corporation (SMC) Award (1997), the Canadian Microelectronics Corporation (CMC) Award (1996), and the Best Student Paper Award in the 1998 Micronet (a Canadian network of centers of excellence on microelectronics) annual workshop. He serves on the technical program committees of several leading IEEE conferences. He is a practicing professional engineer of Ontario, Canada.

Michel S. Nakhla (S'73–M'75–SM'88–F'98) received the M.A.Sc. and Ph.D. degrees in electrical engineering from the University of Waterloo, ON, Canada, in 1973 and 1975, respectively.

From 1976 to 1988, he was a Senior Manager of the Computer-Aided Engineering Group with Bell-Northern Research, Ottawa, ON, Canada. In 1988, he joined Carleton University, Ottawa, ON, Canada, as a Professor and the holder of the Computer-Aided Engineering Senior Industrial Chair established by Bell-Northern Research and the Natural Sciences and Engineering Research Council of Canada. He is currently the Chancellor's Professor of Electrical Engineering at Carleton University. He is the Founder of the high-speed computer-assisted design (CAD) research group at Carleton University. He serves as a technical consultant for several industrial organizations and is the principal investigator for several major sponsored research projects. His research interests include CAD of VLSI and microwave circuits, modeling and simulation of high-speed interconnects, nonlinear circuits, multidisciplinary optimization, thermal and electromagnetic emission analysis, microelectromechanical systems (MEMS), and neural networks.

Dr. Nakhla was Associate Editor of the IEEE TRANSACTIONS ON CIRCUITS AND SYSTEMS—1: FUNDAMENTAL THEORY AND APPLICATIONS and Guest Editor for the IEEE TRANSACTIONS ON COMPONENTS, PACKAGING AND MANUFACTURING TECHNOLOGY: ADVANCED PACKAGING and the IEEE TRANSACTIONS ON CIRCUITS AND SYSTEMS—II: ANALOG AND DIGITAL SIGNAL PROCESSING.